PHYSICAL REVIEW C **88**, 021302(R) (2013)

Local suppression of collectivity in the $N = 80$ isotones at the $Z = 58$ subshell closure

C. Bauer,[1,*] G. Rainovski,[2] N. Pietralla,[1] D. Bianco,[3,4,†] A. Blazhev,[5] T. Bloch,[1] S. Bönig,[1] A. Damyanova,[2,6] M. Danchev,[2] K. A. Gladnishki,[2] T. Kröll,[1] J. Leske,[1] N. Lo Iudice,[3,4] T. Möller,[1] K. Moschner,[5] J. Pakarinen,[7,8] P. Reiter,[5] M. Scheck,[1,‡] M. Seidlitz,[5] B. Siebeck,[5] C. Stahl,[1] R. Stegmann,[1] T. Stora,[7] Ch. Stoyanov,[9] D. Tarpanov,[9] M. J. Vermeulen,[10] D. Voulot,[7] N. Warr,[5] F. Wenander,[7] V. Werner,[11] and H. De Witte[12]

[1]*Institut für Kernphysik, Technische Universität Darmstadt, Darmstadt, Germany*
[2]*University of Sofia, Sofia, Bulgaria*
[3]*Dipartimento di Scienze Fisiche, Università di Napoli "Federico II", Napoli, Italy*
[4]*Istituto Nazionale de Fisica Nucleare, Sezione di Napoli, Napoli, Italy*
[5]*Institut für Kernphysik, Universität zu Köln, Köln, Germany*
[6]*University of Genève, Genève, Switzerland*
[7]*CERN, Genève, Switzerland*
[8]*University of Jyväskylä, Jyväskylä, Finland*
[9]*Institute for Nuclear Research and Nuclear Energy, Bulgarian Academy of Science, Sofia, Bulgaria*
[10]*Department of Physics, University of York, York, United Kingdom*
[11]*WNSL, Yale University, New Haven, Conneticut, United States*
[12]*Instituut voor Kern- en Stralingsfysica, KU Leuven, Leuven, Belgium*

(Received 28 March 2013; published 16 August 2013)

Background: Recent data on $N = 80$ isotones have suggested that the proton $\pi(1g_{7/2})$ subshell closure at $Z = 58$ has an impact on the properties of low-lying collective states.
Purpose: Knowledge of the $B(E2; 2_1^+ \rightarrow 0_1^+)$ value of ^{140}Nd is needed in order to test this conjecture.
Method: The unstable, neutron-rich nucleus ^{140}Nd was investigated via projectile Coulomb excitation at the REX-ISOLDE facility with the MINIBALL spectrometer.
Results: The $B(E2)$ value of 33(2) W.u. expands the $N = 80$ systematics beyond the $Z = 58$ subshell closure.
Conclusions: The measurement demonstrates that the reduced collectivity of ^{138}Ce is a local effect possibly due to the $Z = 58$ subshell closure and requests refined theoretical calculations. The latter predict a smoothly increasing trend.

DOI: 10.1103/PhysRevC.88.021302 PACS number(s): 21.10.−k, 27.60.+j

The mechanism that leads to the formation of nuclear collective states out of the individual motion of many nucleons is one of the major subjects in nuclear structure physics. There are clear relations between the collective properties of even-even nuclei, e.g., the level energies of the first excited 2^+ states and the $B(E2; 2_1^+ \rightarrow 0_1^+)$ transition strengths [1] and the number of nucleons in the valence shell. The global behavior of these quantities between the major shells as a function of the nucleon number is well understood in the frameworks of both collective and microscopic models. One could expect that these general trends in the collective properties between the major shells are modulated by the subshell structure. However, it is usually thought that the pairing correlations with an energy scale of about 2 MeV, smear out and dissolve the subshell structure as long as the separation energies between the subshells are only about a few hundred keV.

The recently observed evolution of the isovector quadrupole-collective valence-shell excitations in the $N = 80$ isotones, the so-called mixed-symmetry states (MSSs) [2], a special class of collective states, suggests that the properties of collective states may be more strongly influenced by the underlying subshell structure than previously thought [3]. In this example there is one single isolated one-phonon $2^+_{1,ms}$ state observed in ^{132}Te [4], ^{134}Xe [5], and ^{136}Ba [6]. This is explained by the consideration that in these isotones the proton excitations mostly happen in the partially filled $g_{7/2}$ orbital, i.e., they are *shell stabilized*. However in ^{138}Ce [3], which has a completely filled $\pi(g_{7/2})$ orbital at $Z = 58$, the formation of one-phonon excitations needs to include a breaking of the subshell closure and thereby the one-phonon MSS fragments suffer from a lack of shell stabilization. MSSs in ^{140}Nd have been investigated in initial works [7,8], which were not conclusive on a possible fragmentation of M1 strength yet. In order to check whether the effect of the $\pi(g_{7/2})$ subshell is also detectable through the properties of the one-phonon fully symmetric 2_1^+ states we have measured the absolute transition strength $B(E2; 2_1^+ \rightarrow 0_1^+)$ in the unstable nucleus ^{140}Nd. Indeed the obtained experimental result reveals a clear deviation of the absolute $B(E2; 2_1^+ \rightarrow 0_1^+)$ strength of ^{138}Ce ($Z = 58$) from the expected collective smooth evolution that implies a relation to the $g_{7/2}$ subshell closure. However, state-of-the-art microscopic models seem unable to reproduce this deviation, which prompts for further theoretical development.

The REX-ISOLDE facility at CERN [9] provided a beam of ^{140}Nd with an energy of 399 MeV, corresponding to

*bauer@ikp.tu-darmstadt.de
†Present address: Ecole Normale Superieur (ENS) de Cachan, Cachan, France.
‡Present address: Department of Engineering, University of the West of Scotland, PA1 2BE Paisley, United Kingdom.

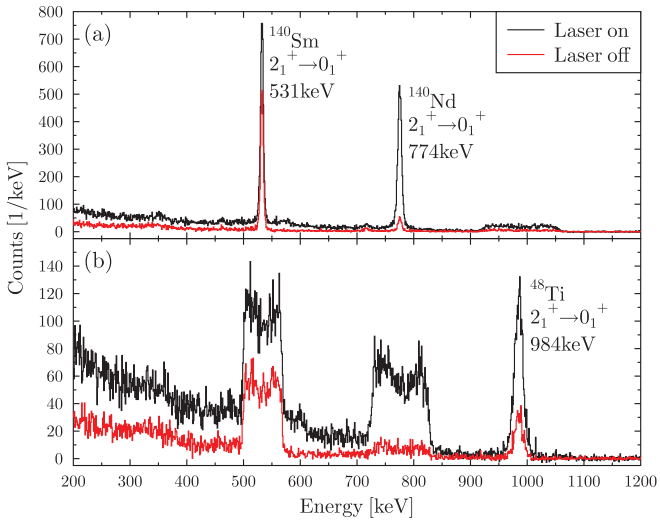

FIG. 1. (Color online) Background-subtracted particle-γ coincidence spectra applying Doppler correction with respect to the (a) projectile or (b) recoiling target nuclei showing the only observed transitions, namely the $2_1^+ \rightarrow 0_1^+$ transitions in ^{140}Sm at 531 keV, in ^{140}Nd at 774 keV and in ^{48}Ti at 984 keV. The unnormalized data with laser ionization switched on (black, 24 h measured time) and off (red, 14 h) are shown on the same scale.

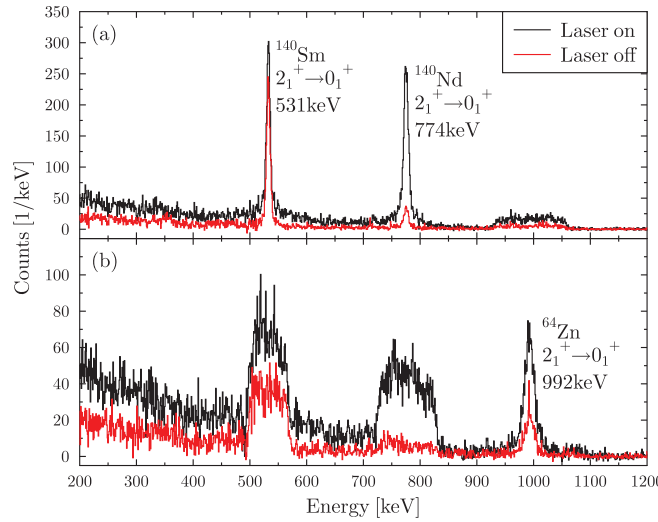

FIG. 2. (Color online) Background-subtracted particle-γ coincidence spectra applying Doppler correction with respect to the (a) projectile or (b) recoiling target nuclei showing the only observed transitions, namely the $2_1^+ \rightarrow 0_1^+$ transitions in ^{140}Sm at 531 keV, in ^{140}Nd at 774 keV and in ^{64}Zn at 992 keV. The unnormalized data with laser ionization switched on (black, 10 h) and off (red, 6 h) are shown on the same scale.

2.85 MeV/u. The ions of interest were produced in a primary target made of tantalum and were extracted using the highly selective laser ionization source RILIS [10,11]. Nevertheless, the beam with a total intensity of 5×10^5 ions/s was contaminated by Sm ions of the same mass (≈50%), which are easily surface ionized. In two subsequent runs the beam impinged on a 1.4 mg/cm^2 ^{48}Ti target and on a 1.55 mg/cm^2 ^{64}Zn target, respectively, for Coulomb excitation. The deexcitation γ rays were detected in the high-purity germanium cluster array MINIBALL covering about 2π of the solid angle [12]. In both cases, mostly targetlike recoiling nuclei were detected in a double-sided silicon strip detector (DSSD) in coincidence with the emitted γ rays. The DSSD was placed in forward direction covering an opening angle of $\theta_{\text{lab}} = 15.6^\circ - 51.8^\circ$ [13]. Figure 1 shows the sum of the γ-ray spectra of all detectors of the MINIBALL array with Doppler correction for mass $A = 140$ projectiles [Fig. 1(a)] and ^{48}Ti target recoils [Fig. 1(b)] in coincidence with the particle signals from the DSSD. No other γ-ray transitions than the deexcitation of the 2_1^+ states to the ground states at 531 keV for the ^{140}Sm contamination, at 774 keV for ^{140}Nd and at 984 keV for ^{48}Ti were visible. In the case of the ^{64}Zn target (cf. Fig. 2) instead of the transition in ^{48}Ti the deexcitation of the Coulomb-excited 2_1^+ state in ^{64}Zn is visible at almost the same energy (992 keV).

The Coulomb excitation cross section for the 2_1^+ state of ^{140}Nd was measured relative to the known cross sections of the target excitations. A crucial point in this kind of experiment with a radioactive beam is the determination of the beam contaminants. In this experiment an isobaric contamination of ^{140}Sm was observed. It was possible to determine the contribution of the ^{140}Sm contaminant to the target excitation yield by performing runs with and without laser ionization. Figures 1 and 2 show the Doppler-corrected and background-subtracted spectra with the laser switched on (black) and off (red). The laser settings were optimized for ionizing Nd isotopes, such that the Nd excitation is suppressed for runs without the laser. The amount of Sm in the beam is not affected by the laser and can thereby serve for normalizing the spectra to the Sm contaminant. By subtracting the normalized laser-off spectrum a pure Coulomb excitation spectrum of Nd on either the Ti or the Zn target is obtained. Through this procedure one assures that the remaining target excitation yield is correlated to the yield of the Nd excitation and not to any other beam components. We have verified that the same result can also be achieved by normalizing the laser-on and laser-off spectra to the total time they have been collected for. The results are identical and here we present only the γ-ray yields N_γ/ϵ_γ obtained by normalizing the spectra to the Sm contaminant. The measured yields, i.e., γ-ray peak areas divided by relative detection efficiencies, are summarized in Tables I and II.

The Coulomb excitation cross section σ for the 2_1^+ state is influenced by both the transitional and the diagonal matrix elements, M_{20} and M_{22}. Using the multiple Coulomb excitation code GOSIA2 [14] these matrix elements are varied such that the experimental γ yields (compare Tables I

TABLE I. Summary of the measured γ-ray yields in the ^{48}Ti(^{140}Nd,^{140}Nd*)^{48}Ti* reaction for the different ranges of scattering angles (corrected for relative γ-ray efficiency).

θ_{lab} range	Ring (DSSD)	Detected	^{140}Nd	^{48}Ti
27.8°–33.0°	4–5	Target	565(24)	217(17)
37.8°–45.6°	8–11	Target	1346(53)	531(27)
45.7°–51.8°	12–15	Target	1221(36)	547(27)

TABLE II. Summary of the measured γ-ray yields in the ^{64}Zn(^{140}Nd,^{140}Nd*)^{64}Zn* reaction for the different ranges of scattering angles (corrected for relative γ-ray efficiency).

θ_{lab} range	Ring (DSSD)	Detected	^{140}Nd	^{64}Zn
33.1°–43.8°	6–10	Target	464(22)	239(18)
43.9°–51.8°	11–15	Target	515(23)	211(17)
15.6°–24.8°	0–2	Projectile	1281(36)	492(26)

and II) are reproduced. The mutual dependence of the projectile's excitation cross section σ^P on M_{20} and M_{22} results in an area in the (M_{22}, M_{20}) plane representing the experimental Coulomb excitation cross section. The projectile excitation is normalized to the target-excitation cross section σ^T of the 2_1^+ state of ^{48}Ti, respectively ^{64}Zn, taking also the angular distribution $W(\theta_\gamma)$ of the γ rays, including deorientation, into account,

$$\sigma^P(M_{20}, M_{22}) = \frac{N_\gamma^P}{N_\gamma^T}\frac{\epsilon_\gamma^T}{\epsilon_\gamma^P}\frac{W(\theta_\gamma)^T}{W(\theta_\gamma)^P}\sigma^T. \quad (1)$$

Superscripts P and T denote quantities related to the projectile and target excitation, respectively. The main contributions to the uncertainty are the statistical errors of the experimental γ-ray yields N_γ from projectile (^{140}Nd) and target excitation (^{48}Ti/^{64}Zn), as well as the uncertainties in the matrix elements of the target nuclei. The relative efficiencies of the germanium detectors at the transition energies is denoted by ϵ. Their ratio in Eq. (1) has an error of approximately 1–2%. In order to maximize the sensitivity and simultaneously keep the statistical error at a reasonable level, different scattering-angle regimes were defined. For the run with the ^{48}Ti target, the targetlike recoils with scattering angles $\theta_{lab} = 27.8°$–$33.0°$, $37.8°$–$45.6°$, $45.7°$–$51.8°$ have been selected, which each correspond to several rings of the DSSD. Due to the different kinematics the ranges have been adjusted for the ^{64}Zn target (cf. Table II).

A fixed set of start parameters for the matrix elements M_{20} and M_{22} is given as input to the GOSIA2 program, which then calculates γ-ray yields from Coulomb-excitation theory. By comparison to the experimental yields a χ^2 value is obtained for each set of initial start parameters M_{20} and M_{22}. The variation of these start parameters results in a χ^2 surface plotted in Fig. 3. The 1σ contour of this surface is projected to the respective axis to extract the matrix elements and their uncertainties. The experimental results of the χ^2 surface

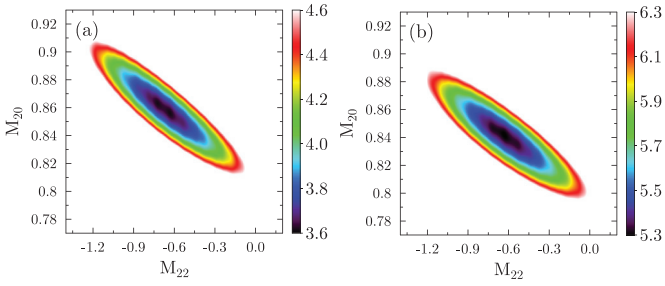

FIG. 3. (Color online) χ^2 surface with respect to the diagonal and transitional matrix elements of the 2_1^+ state in ^{140}Nd from the Coulex experiment with (a) ^{48}Ti and (b) ^{64}Zn target.

TABLE III. Summary of the experimental results for the 2_1^+ state in ^{140}Nd for the single runs with Ti/Zn target and a weighted average.

	M_{20} [eb]	$B(E2)\uparrow$ [e^2b^2]	M_{22} [eb]	$Q(2_1^+)$ [eb]
^{48}Ti target	0.860(47)	0.74(8)	−0.65(57)	−0.49(43)
^{64}Zn target	0.842(46)	0.71(8)	−0.62(58)	−0.47(44)
Weighted average	0.85(3)	0.72(5) =33(2) W.u.	−0.64(41)	−0.48(31)

projections and the deduced observables are summarized in Table III.

We have compared the experimental results to two different microscopic calculations, the quasiparticle phonon model (QPM) and large-scale shell-model (LSSM) calculations. The QPM [15] treats a Hamiltonian of separable form in a microscopic multiphonon basis built of phonons generated in the quasiparticle random-phase approximation (QRPA) [16,17]. It is therefore capable of describing the anharmonic features of collective modes as well as multiphonon excitations. Since the constituent phonons include two quasiparticle states covering a very large energy spectrum, it is possible to use effective charges very close to the bare values ($e_\pi = 1.05$ and $e_\nu = 0.05$). The Hamiltonian parameters used here are the same ones adopted in a previous calculation [18] to optimize the description of the fully symmetric states (FSS) and MSSs of the $N = 80$ chain up to $Z = 58$. The calculation has therefore a predictive power for $^{140}_{60}$Nd.

The LSSM adopts a model space in which the valence protons and neutrons, treated respectively as particles and holes external to a $Z = 50$ and $N = 82$ core (^{132}Sn), are distributed among the shells $\{2d_{5/2}, 1g_{7/2}, 2d_{3/2}, 3s_{1/2}, 1h_{11/2}\}$. The calculations use a realistic two-body Hamiltonian (a renormalized G matrix derived from the CD-Bonn potential) with the same single-particle (hole) energies adopted for the Xe isotopes [19]. More specifically, the neutron-hole energies were taken from the levels of ^{135}Xe, while the proton energies were the same adopted to study the spectra of ^{108}Sn and ^{133}Xe [20]. Thus, the LSSM calculations are completely parameter free and fully predictive for the whole $N = 80$ chain. They are also exact within the 0-$\hbar\omega$ model space adopted. On the other hand, the shell-model space does not include high-energy and core excitations, whose effects are incorporated into the effective charges $e_\pi = 1.6$ and $e_\nu = 0.7$, the same adopted for the Xe isotopes [19].

The parameters of both models have been adapted to the description of other nuclei than ^{140}Nd for which their results can be considered as predictions. The QPM as well as the shell-model calculations provide a good agreement of the excitation energies for the 2_x^+ states of ^{140}Nd (cf. Fig. 4) including the suspected 2_{ms}^+ states [7,8]. The general trend of growing $B(E2; 2_1^+ \rightarrow 0_1^+)$ strength in the $N = 80$ isotones moving away from the $Z = 50$ shell closure as shown in Fig. 5 is expected due to the increase in collectivity when adding more and more valence protons N_π. However, the QPM predicts a smaller $B(E2; 2_1^+ \rightarrow 0_1^+)$ value of 21 W.u. compared to the experimentally found value of 33(2) W.u.

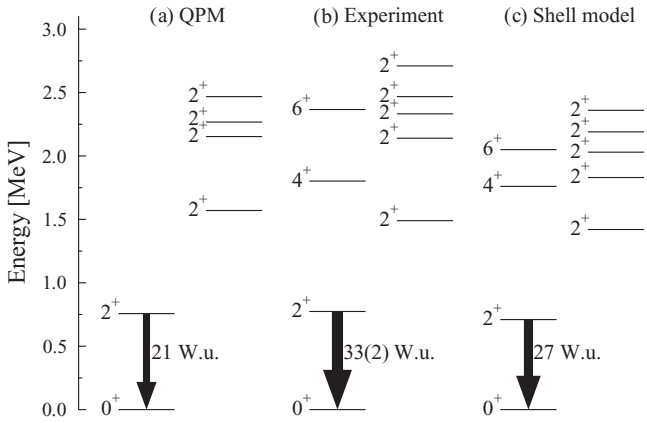

FIG. 4. The experimental level scheme for ^{140}Nd is shown (b) together with the calculated ones from the (a) QPM and (c) shell model [21]. The illustration concentrates on the 2^+_x states.

The shell-model calculations predict a strength of 27 W.u. but still below the measured value. Both calculations describe a smoother increase than what the data suggest. They are in agreement with the smaller $B(E2)$ value for ^{138}Ce, but they do not reproduce the larger value for ^{140}Nd. Ignoring the $B(E2)$ value for ^{138}Ce all other experimental values, including the one for ^{140}Nd, seem to increase almost linearly. Regarding the quadrupole moment the outcome of the shell-model calculations is $Q(2^+_1) = +0.26e$b. Although the experimental result ($Q = -0.48(31)e$b) has the opposite sign the absolute values are small, which agrees with the general observation of rather spherical shapes in the proximity of shell closures ($N = 82$).

The near-linear behavior of the $B(E2)$ values can be understood as a simple scaling with valence-proton number. The $N_\pi N_\nu$ valence correlation scheme from Casten and Zamfir [25] describes the linear increase of collectivity with $N_\nu = 2$ (2 valence neutron holes) and $N_\pi = 0, 2, 4, \ldots$ for the protons.

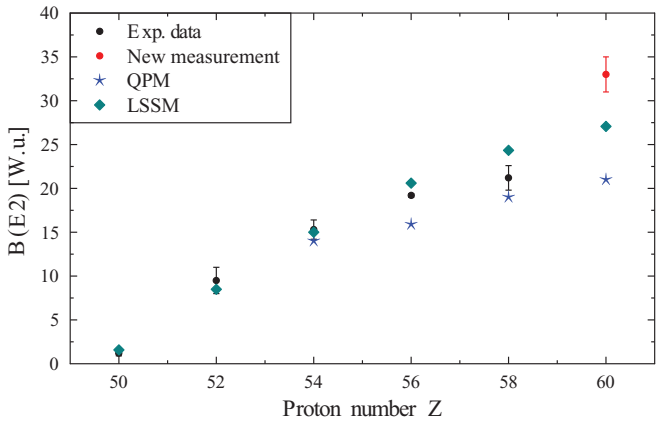

FIG. 5. (Color online) Systematics of $B(E2)$ values in W.u. for the first excited 2^+_1 states in the even $N = 80$ isotones from $Z = 50$ (Sn) to $Z = 60$ (Nd). The existing experimental data [1,4,22–24] including the extracted value for ^{140}Nd are presented in comparison with the large-scale shell-model calculations [21] as well as the quasiparticle phonon model [18].

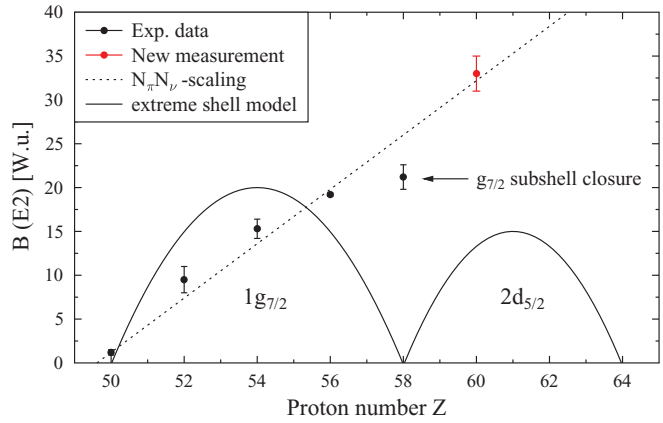

FIG. 6. (Color online) Systematics of $B(E2)$ values in W.u. for the first excited 2^+_1 states in the even $N = 80$ isotones covering the range of the $\pi g_{7/2}$ and $\pi d_{5/2}$ orbitals. The existing experimental data is presented as in Fig. 5 with a schematic illustration of a linear $N_\pi N_\nu$ dependence (dashed) and an extreme shell model case (solid lines).

In that approach nuclear data is parameterized to explicitly emphasize the valence *p-n* interaction. It is assumed that the onset of collectivity, configuration mixing, and deformation in nuclei is solely due to the *p-n* interaction. This interaction is fairly long ranged, orbit independent, and relevant only for the valence protons and neutrons. These extreme assumptions, averaged over many valence nucleons, have proven to be reasonable. By applying this scheme to the $N = 80$ isotones we obtain a consistent description of the experimental data except for $Z = 58$ as indicated by the dashed line in Fig. 6. The single-particle degrees of freedom are accounted for only through the number of valence bosons, which is known to be a limited approximation. On the other hand data on the one-phonon MSSs strongly suggest that the single-particle degrees of freedom can influence the collective properties dramatically at least for the MSSs through the shell stabilization effect [3].

In an extreme shell-model scenario, considering the valence protons to occupy only the $\pi(g_{7/2})$ orbit, the $B(E2)$ strength vanishes at $Z = 50$ and $Z = 58$ and it has a maximum at midsubshell, indicated by the solid curves in Fig. 6. The experimental data can be interpreted as a convolution of the both presented extreme scenarios. The suppression of the transition strength in ^{138}Ce with respect to the $N_\pi N_\nu$ behavior is considered as originating from the $Z = 58$ subshell closure. However, this local suppression of $B(E2)$ strength in ^{138}Ce is not seen in the shell-model calculations. Such a quenching might be the outcome of a subtle competition between the single-particle energy levels, responsible for the gap between different subshells, and the two-body correlations, especially pairing, which tend to smooth out the effects of the subshell structure. This hypothesis, suggested by the extreme shell-model picture, can be tested by fine tuning the single-particle levels used in the LSSM calculations [19] so as to counterbalance the smoothing action of pairing. Alternatively, one may surmise that the core polarization produces smaller effective charges in correspondence of a subshell closure. In order to test such a suggestion, one should compute explicitly the effective $E2$ operators within the linked cluster expansion theory, which

is known to generate different effective charges for different subshells [26]. However, it was pointed out [19,21] that a calculation in an enlarged shell-model space, which includes core excitations, is not feasible.

In summary, the measured $B(E2; 2_1^+ \rightarrow 0_1^+)$ value of 33(2) W.u. in ^{140}Nd is compared to recent large-scale shell-model calculations [21] as well as to the quasiparticle phonon model in connection to the systematics of the $N = 80$ isotones [18,21]. In both models, the computed $B(E2)$ strengths in the stable $N = 80$ isotones increase smoothly with Z. This trend is consistent with the experiments apart from some deviations in the heavier isotones, where the measured data do not have a smooth behavior. In fact, the $E2$ transition is suppressed to some extent in ^{138}Ce and enhanced in ^{140}Nd. Such an anomalous behavior is ascribed to the filling of the $\pi(g_{7/2})$ subshell for $Z = 58$. However, this shell effect is neither reproduced by the QPM, which tends to systematically underestimate the strength, nor by the LSSM, which yields a larger $B(E2)$ value for ^{138}Ce and a smaller one for ^{140}Nd. These discrepancies may be cured within the shell model by a more refined treatment of the single-particle energies capable of inducing a more pronounced subshell structure or by explicitly taking into account the excitations of the core.

We gratefully acknowledge the support of the staff members at CERN during the experimental runs, in particular Emiliano Piselli and Miguel Benito, furthermore Adam Hayes for his help regarding the GOSIA computer code. This experiment was supported by the BMBF under Grants No. 05P09RDCI6, No. 05P12RDCIB, No. 06DA9036I, No. 05P12RDCIA, No. 05P09PKCI5, No. 05P12PKFNE, and No. 06KY9136I, HIC for FAIR funded by the State of Hesse in the framework of the LOEWE program, the DAAD German-Bulgarian exchange program under Grants No. PPP 50751591 and No. DNTS/01/2/2011, U.S. DOE Grant No. DE-FG02-91ER-40609, ENSAR, and by a Marie Curie Intra-European Actions grant of the European Community's 7th Framework Programme under Contract No. PIEF-GA-2008-219175.

[1] S. Raman, C. Nestor, Jr., and P. Tikkanen, At. Data Nucl. Data Tables **78**, 1 (2001).
[2] F. Iachello, Phys. Rev. Lett. **53**, 1427 (1984).
[3] G. Rainovski, N. Pietralla, T. Ahn, C. J. Lister, R. V. F. Janssens, M. P. Carpenter, S. Zhu, and C. J. Barton, Phys. Rev. Lett. **96**, 122501 (2006).
[4] M. Danchev *et al.*, Phys. Rev. C **84**, 061306 (2011).
[5] T. Ahn, L. Coquard, N. Pietralla, G. Rainovski, A. Costin, R. Janssens, C. Lister, M. Carpenter, S. Zhu, and K. Heyde, Phys. Lett. B **679**, 19 (2009).
[6] N. Pietralla *et al.*, Phys. Rev. C **58**, 796 (1998).
[7] E. Williams, R. J. Casperson, V. Werner, H. Ai, P. Boutachkov, M. Chamberlain, G. Gürdal, A. Heinz, E. A. McCutchan, J. Qian, and R. Winkler, Phys. Rev. C **80**, 054309 (2009).
[8] K. A. Gladnishki *et al.*, Phys. Rev. C **82**, 037302 (2010).
[9] O. Kester *et al.*, Nucl. Instrum. Methods Phys. Res. B **204**, 20 (2003).
[10] V. Fedosseev *et al.*, Nucl. Instrum. Methods Phys. Res. B **266**, 4378 (2008).
[11] F. Schwellnus *et al.*, Nucl. Instrum. Methods Phys. Res. B **267**, 1856 (2009).
[12] N. Warr *et al.*, Eur. Phys. J. A **49**, 40 (2013).
[13] A. Ostrowski, S. Cherubini, T. Davinson, D. Groombridge, A. Laird, A. Musumarra, A. Ninane, A. di Pietro, A. Shotter, and P. Woods, Nucl. Instrum. Methods Phys. Res. A **480**, 448 (2002).
[14] T. Czosnyka, D. Cline, and C. Wu, Bull. Am. Phys. Soc. **28**, 745 (1983).
[15] N. Lo Iudice, V. Y. Ponomarev, C. Stoyanov, A. V. Sushkov, and V. V. Voronov, J. Phys. G: Nucl. Part. Phys. **39**, 043101 (2012).
[16] D. Rowe, *Nuclear Collective Motion: Models and Theory* (World Scientific, Singapore, 2010).
[17] P. Ring and P. Schuck, *The Nuclear Many-Body Problem*, Texts and Monographs in Physics (Springer, Berlin, 2005).
[18] N. Lo Iudice, C. Stoyanov, and D. Tarpanov, Phys. Rev. C **77**, 044310 (2008).
[19] D. Bianco, F. Andreozzi, N. Lo Iudice, A. Porrino, and F. Knapp, Phys. Rev. C **84**, 024310 (2011).
[20] F. Andreozzi, N. Lo Iudice, and A. Porrino, J. Phys. G: Nucl. Part. Phys. **29**, 2319 (2003).
[21] D. Bianco, F. Andreozzi, N. Lo Iudice, A. Porrino, and F. Knapp, Phys. Rev. C **85**, 034332 (2012).
[22] D. Radford *et al.*, Nucl. Phys. A **746**, 83 (2004).
[23] G. Jakob *et al.*, Phys. Rev. C **65**, 024316 (2002).
[24] M. J. Bechara, O. Dietzsch, and J. H. Hirata, Phys. Rev. C **29**, 1672 (1984).
[25] R. F. Casten and N. V. Zamfir, J. Phys. G: Nucl. Part. Phys. **22**, 1521 (1996).
[26] N. Lo Iudice, D. Rowe, and S. Wong, Nucl. Phys. A **219**, 171 (1974).